

## Microwave Resonators for Weak Light Detection at Telecom Wavelength

Pin-Jia Zhou<sup>1</sup>, Yiwen Wang<sup>1</sup>, Qiang Wei<sup>1</sup>, and Lian-Fu Wei<sup>1, 2, \*</sup>

**Abstract**—We report the experimental measurements of weak light signal at 1550 nm wavelength with a high-quality factor microwave coplanar waveguide (CPW) resonators. The quality factor of this niobium  $\lambda/4$  CPW resonator is measured as  $Q = 7.4 \times 10^5$  at ultra-low temperature (20 mK). With this device, we developed a technique to implement the proper fiber-resonator coupling, and realized the desirable weak light detection at telecommunication wavelength with 35 pW resolution by probing the shift of resonance frequency ( $f_0$ ). We found that the resonator shift increases with the increasing light power (from 11.7 pW to 9.77 nW), similar to the effects of increasing the system temperature (from 20 mK to 800 mK). The observed blue shifts of  $f_0$  (with the increasing of either the temperature and the applied light powers) are thoroughly deviated from the usual Mattis-Bardeen theory prediction, and could be explained by the effects relating to the two-level system existed on surface of the CPW device.

### 1. INTRODUCTION

Ultra sensitive photon number resolving detectors (PNRDs), which can determine the number of photons in a light pulse, are currently attracting substantial interests [1], particularly for optical quantum communications [2, 3] and optical quantum information processings [4]. Superconducting detectors, including superconducting nanowire detectors [5], superconducting tunnel junctions [6], and transition-edge sensors (TES) [7], etc., show great prospects in these applications. For instance, film tungsten TESs have been reported over 95% quantum efficiency and photon-number resolving ability at 1550 nm [8]; also, the reported bulk titanium TESs have shown  $98\% \pm 1\%$  detection efficiency at 850 nm [2]. Alternatively, another kind of superconducting microwave detector based on coplanar waveguide technique, typically the coplanar waveguide resonators (CPWs), have also promptly developed for sensitive detections of radiations (from submillimeter to x-ray [9] and gamma ray [10]) in astronomic applications. Typically, CPW detector works within the GHz wave band, and possesses two main advantages: i) the fabrication is relatively simple (since the CPW device normally consist of one thin film layer which deposited on a silicon or sapphire substrate), and ii) the scalability is more obvious (they are convenient to multiplex as a large array, can be operated simultaneously with only one wide-band amplifier and readout via one commercial electronics system [11]).

Physically, quasiparticles can be created in the CPW resonator when it absorbs the incident radiation energy. This will change the surface impedance of the superconducting strips. Therefore, the desired radiation detection can be achieved by using a relatively-simple technique (via monitoring the change of central frequency and phase shift of the  $|S_{21}|$  characteristic curves). Based on the Mattis-Bardeen Theory (MBT) [12], the increase of quasiparticle density will both increase the surface impedance  $Z_s = R_s + i\omega L_s$  (with  $R_s$  is the surface resistance and the  $L_s$  is the surface inductance) [13]. As a consequence, the measured resonant frequency of the CPW will decrease due to the increased  $L_s$ ,

---

Received 3 May 2014, Accepted 4 August 2014, Scheduled 15 August 2014

\* Corresponding author: Lian-Fu Wei (weilianfu@gmail.com).

<sup>1</sup> Quantum Optoelectronics Laboratory, Southwest Jiaotong University, Chengdu 610031, P. R. China. <sup>2</sup> State Key Laboratory of Optoelectronic Materials and Technologies, School of Physics and Engineering, Sun Yat-Sen University, Guangzhou 510275, P. R. China.

and the quality factor ( $Q$ ) of the resonator will decrease due to the increased  $R_s$ . These effects have been verified in the previous CPW experiments, wherein the measurements are achieved near the critical temperature of the resonator [14, 15].

In this paper, we report the experimental observations with a high- $Q$  niobium CPW resonator working far below its superconducting critical temperature. The observed results are manifestly deviated from the predications of MBT. Our device is a  $\lambda/4$  CPW resonator with a sufficiently high quality factor (i.e.,  $Q = 7.4 \times 10^5$  measured at 20 mK). By probing the central frequency shifts of the resonator under light radiations, we achieve the desired weak light detection, i.e., evident resolution of weak power is 35 pW. Particularly, we observed that the resonant frequency of the measured CPW increases with the increasing temperature and also the increasing incident light power. Obviously, if the light incidence events can be seemed equally to the increasing temperature effects, then our observations should be essentially different from those phenomena observed in the experiments with the Tantalum- and Tungsten-Silicide-alloy resonators [14, 15] (where the measured resonance frequencies of the resonator decrease with the increasing temperature). Our results, deviated from the MBT, could be explained by the effects related to two-level systems existing on top of the resonator surface [16].

## 2. DEVICES AND MEASUREMENT SYSTEM

### 2.1. Microwave Coplanar Waveguide Resonator

The resonator consists of a coplanar waveguide with a length of  $15.814 \text{ mm} = \lambda/4$ , where  $\lambda$  is the wavelength of the microwave resonance in the resonator. The length  $l$  relates to the resonant frequency  $f_0$ , the light speed  $c$ , and the effective dielectric constant  $\epsilon_{eff} = (\epsilon_r + 1)/2$  as [17],

$$l = \frac{c}{4f_0\sqrt{\epsilon_{eff}}} = \frac{c}{4f_0}\sqrt{\frac{2}{\epsilon_r + 1}} \quad (1)$$

where  $\epsilon_r$  is the relative permittivity of the substrate. This resonator is a 160 nm-thick niobium film on a 500 nm-thick high-resistivity ( $> 10 \text{ k}\Omega\text{-cm}$ ) silicon substrate. A layout structure of the resonator is shown in Fig. 1, where perfectly sharp border between the transmission line and the ground plate is seen [17].

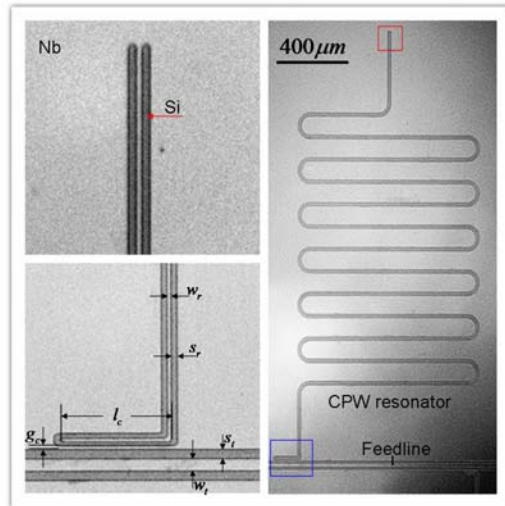


**Figure 1.** A microscope structure of our Niobium CPW resonator. The device (lighter gray part) is deposited on a high-resistivity silicon substrate (dark gray part). Left part of the figure illustrates the enlargement configurations of the coupler elbow (lower section, blue rectangular) and the grounding end of the resonator (upper section, red rectangular) joined in ground plate. The center strip width  $w_r$  is  $7 \mu\text{m}$  and the center strip gap  $s_r$  is  $5 \mu\text{m}$ , the coupling elbow has a scale of  $80 \mu\text{m}$  length ( $l_c$ ) with a  $g_c=5 \mu\text{m}$  gap, and the feedline width  $w_t = 20 \mu\text{m}$  and  $s_t = 15 \mu\text{m}$ .

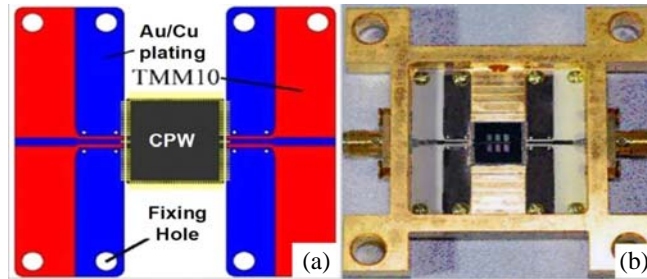


**Figure 2.** The layout of the carefully designed PCB in our experiments. (a) The simulated structure in HFSS software, red part stands for the TMM10 base substrate and blue part stands for the Au-plating region. (b) The sample box with real PCB and CPW fixed in the center.

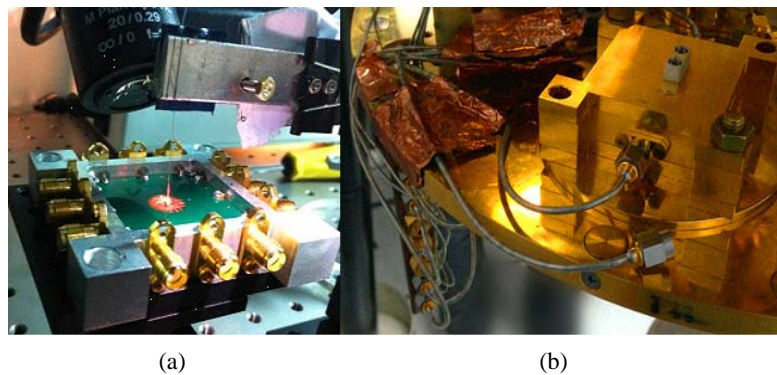


**Figure 3.** (a) shows a claw which holds the fiber tail for manually calibrating in room temperature. The CPW is glued in center of the gold-plate oxygen-free copper sample box, which is fixed on the table (to avoid unwanted vibrations). (b) shows two of the eight coaxial cables on mixing chamber plate inside the dilution refrigerator.

The device is glued with GE varnish inside a gold-plated copper sample box. Between the connectors of the box and the resonator, a Print Circuit Board (PCB) is installed to assure the characteristic impedance matching, i.e.,  $Z_0 = 50 \Omega$  (in order to reduce the signal reflections). Choosing the PCB material should carefully consider several standards including the low thermal coefficient of dielectric constant, low thermal expansion and high thermal conductivity [18, 19]. In our experiment, we use the TMM10 laminates (its dielectric constant is 9.2) produced by Rogers corporation as the base substrate, and the connecting sections are covered by the Au plating copper layer, shown in Fig. 2(a). The width of transmission line is set as 1 mm and 600  $\mu\text{m}$  respectively in the TMM10 and Au-plating part for characteristic impedance matching. When the PCB has fixed in the sample box, aluminum bonding wires will join the side of PCB to ground plate of the resonator to suppress various unwanted transmission modes (which could cause excess leakage of the microwave signals) [20], shown as Fig. 2(b). Then, weak light signals couple to the resonator through a standard 9  $\mu\text{m}$  core single-mode tail telecommunication fiber. Once the fiber is adjusted above the ground end of the  $\lambda/4$  resonator, a clamp is used to fix the fiber to minimize the movement from the alignment region. Also, to increase the fiber-resonator coupling efficiency, the space gap between the exit fiber end and the film surface is filled with an drop of ultraviolet-curable resin, shown in Fig. 3(a).

## 2.2. Ultra-Low Temperature Measurement System

Testing the transmission characteristics through the microwave CPW resonator used for weak light detection requires an ultra-cold environment; the temperature should be 10% of the superconducting transition temperature  $T_c$ . This is achieved in our experiment by using a dilution refrigerator (DR) which base temperature is  $\sim 20$  mK.

We used two stainless steel coaxial cables and one telecommunication single-mode optical fiber to bring the microwave and the weak light (with the wavelength of 1550 nm) signals from room temperature to the sample plate, respectively. The input microwave signal produced from an Agilent Vector Network Analyser (VNA) goes through a standard SMA (subminiature version A) connector, an attenuator, a DC blocker and eventually transmit through the resonator. The unwanted excess noise and low frequency noise, caused from the vibrations of rotary valve, have been suppressed effectively. The weak light signal emits from the laser source transporting along the telecommunication fiber through a variable attenuator, a spectrometer and then radiates on the resonator grounded end. The aggregate power attenuation of the fiber (without any controlled attenuator) is measured as  $-43$  dBm. Fig. 4 shows the whole cabling conformation for the present weak light detection with a microwave CPW resonator.

### 3. EXPERIMENTAL RESULTS

We perform the microwave transmission measurements of the resonator under the ultra-low temperature condition, i.e., during the measurements the system temperature is kept below 800 mK. In order to keep the resonator working in its superconducting state and working well as a weak light detector, the power of the applied light is attenuated properly.

#### 3.1. Microwave Transport Features of the Resonator without Light Irradiation

At around 20 mK base temperature of the DR, we measured the microwave transport characteristics  $|S_{21}|$  curves of the CPW using the connected vector network analyzer (VNA) with a  $-48$  dBm driving power. As the  $\lambda/4$  resonator will reflect the signals at its resonant points, the resonant feature of the  $S_{21}$  parameter through the VNA should be a series of narrow dips, showing the frequency-dependent feature of the measured superconducting resonator. Experimentally, we found a few resonant dips corresponding respectively to the relevant resonant modes. For example, the first dip corresponds to the fundamental mode of the resonator (i.e.,  $\lambda/4$ ) and the second dip marks the first excited mode (i.e.,  $3\lambda/4$ ). For the present resonator the center frequency and quality factor of the first dip were measured as  $f_1 = 1.8361$  GHz (only deviated 1.2 MHz from the designed value of 1.8473 GHz),  $Q_1 = 7.4 \times 10^5$ , and the parameters for the second dip are  $f_2 = 5.5018$  and  $Q_2 = 7.0 \times 10^5$ . Limited by the inevitable noises, the quality factors at the higher resonant frequencies (not shown here) are significantly low. Above, the center frequency  $f_0$  is defined as the frequency value corresponding to the lowest point of the relevant dip, and the quality factor  $Q$  is determined by the formula  $Q = f_0/\Delta f$  with  $\Delta f$  being the  $-3$  dB bandwidth. Also, for the equivalent  $-48$  dBm microwave driving signals, the system attenuations for the first- and the second dips are approximately  $-15$  dB and  $-29$  dB, respectively.

#### 3.2. Light Irradiation Responses of Superconducting Resonators at Low Temperature

The desired weak light detection is implemented simply by probing the shifts of the center frequencies of the dips. In our experiment, the 1550 nm consecutive diode laser with controllable power is introduced via a 9  $\mu\text{m}$ -core optical single-mode fiber, illuminating on the surface of the microwave resonator in the sample box. The power  $P$  of the light irradiating on the resonator is monitored by a sensitive power meter, which is put in a dark box to avoid extra light disturbance. In the experiments, the irradiation power  $P$  (with the unit of *watt*) of the light is usually represented as the equivalent power  $P'$  (with the unit of *dBm*):  $P' = 30 + 10 \lg P$ . Also,  $P'$  is controllable via an adjusted light attenuator.

The shifts of center frequencies for the first and second dips shown in Fig. 4(a) and Fig. 4(b), respectively. The black lines mark the  $|S_{21}|$  transport features both without the light irradiation. Instead, the colored lines represent the responses of the dips to the light irradiations. Specifically, in order to probe how the first dip changes with the light irradiation, we firstly switch on the laser source and then slowly decrease its irradiation power on the resonator from  $-50.1$  dBm to  $-79.3$  dBm. The experimental results show that the central frequency of the first resonant dip decrease from 1.8361538 GHz to 1.8361492 GHz. This indicates that, with the decrease of the applied power  $P'$ , the central frequency at this dip shifts weakly from that without the light irradiation. Indeed, for the initially applied power  $P' = -50.1$  dBm, the shift of the center frequency is measured as  $+4.6$  kHz (see the blue line in Fig. 5(a)). Also, for a sufficiently weak light signal with  $P' = -73.3$  dBm (i.e.,  $P = 46.7$  pw)

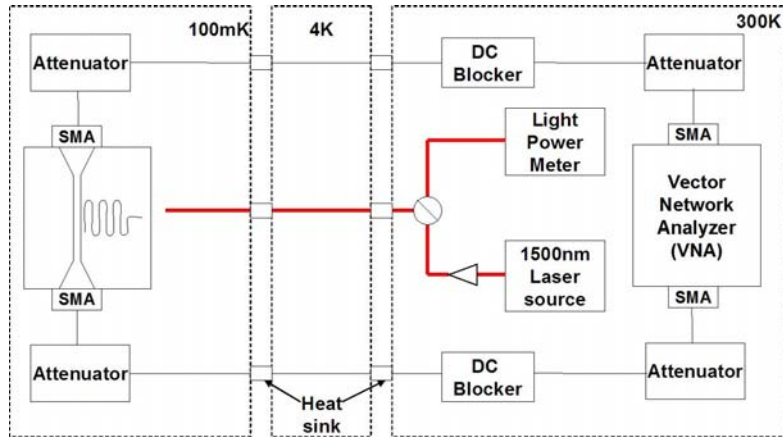


**Figure 4.** Cables conformation of the our measurement system. The red line indicates the telecommunication single-mode optical fiber which transports the 1550 nm laser signal from room temperature to the low temperature circumstance. The inletting light energy is monitored by using a keen light power meter instantaneously via a spectrometer (represented by the round circle). The triangle stands for a variable power attenuator to adjust the power (from  $-36$  dBm to  $-7$  dBm) of the laser radiating on the resonator.

a shift with  $+300$  Hz of the center frequency is still detected (the red line in Fig. 5(a)). When further decrease the power to  $P' = -79.3$  dBm (i.e.,  $P = 11.69$  pW) we find that the dip is overlapped to the condition without light irradiation (i.e., the black line in Fig. 5(a)). These measurements imply that, using such a dip detection technology, the weak 1550 nm light signal with power  $P \approx 35$  pW can be detected. Similarly, power-to-frequency dependency is also measured by probing the changes in the second resonant dip. The relevant results are schematized in Fig. 5(b). It is seen that this dip can only respond to the signal with the power  $P' \geq -62.32$  dBm (i.e.,  $P \geq 5.86 \times 10^{-1}$  nW). In addition, with the same  $+300$  Hz frequency resolution, the smallest detectable power is 194.4 pW, which is approximately 5 times larger compared with the measurement of the first resonant dip.

We also measured how the loaded quality factor of the resonator changes with the increasing irradiating power. The results are shown in Fig. 6, i.e.,  $\Delta f/f_0 = [f(P) - f_0]/f_0$  and the quality factor  $Q$  versus the powers of the irradiating light are schematized in Fig. 6(a) for the first dip and Fig. 6(b) for the second dip, respectively. Here,  $f(P)$  represents the measured center frequencies of the changed dips and  $f_0$  is the center frequency of the relevant dip without light irradiation. It is seen from the Fig. 6, the light-dependent behaviors of center frequency shifts and  $Q$ -factor variations for the dips are roughly the same, i.e., with the increase of the irradiation power the center frequency shift increases while the quality factor decreases. However, these behaviors still exist manifest quantitatively difference. This can be seen from the magnitudes of the relatively center frequency shifts  $\Delta f/f_0$ , the magnitude for the first dip is almost one order larger than that for the second dip. This verifies again that the sensitivity for the weak light detection by probing the change of the first dip is more accurate than using the second dip. The red lines in illustrations represent the loaded quality factor versus the increased radiation power. It is seen clearly that the quality factors for the two dips decrease with the increase of the applied power. Physically, this is attributed to the enhancing dissipation of the resonator due to stronger light power.

### 3.3. Irradiation Saturate Temperatures of Superconducting Resonators for Weak Lights

The measurement results demonstrated above show clearly that, with the enhanced energy absorption due to light irradiation, the center frequencies of the dips increase and their quality factors decrease. Given the microwave transport parameters measured by the VNA (i.e., the center frequency and the loaded quality factor of the dips) are the entire property of the resonator, we believe that the similar change of the dips (due to the light irradiation) can also be found by adjusting the system

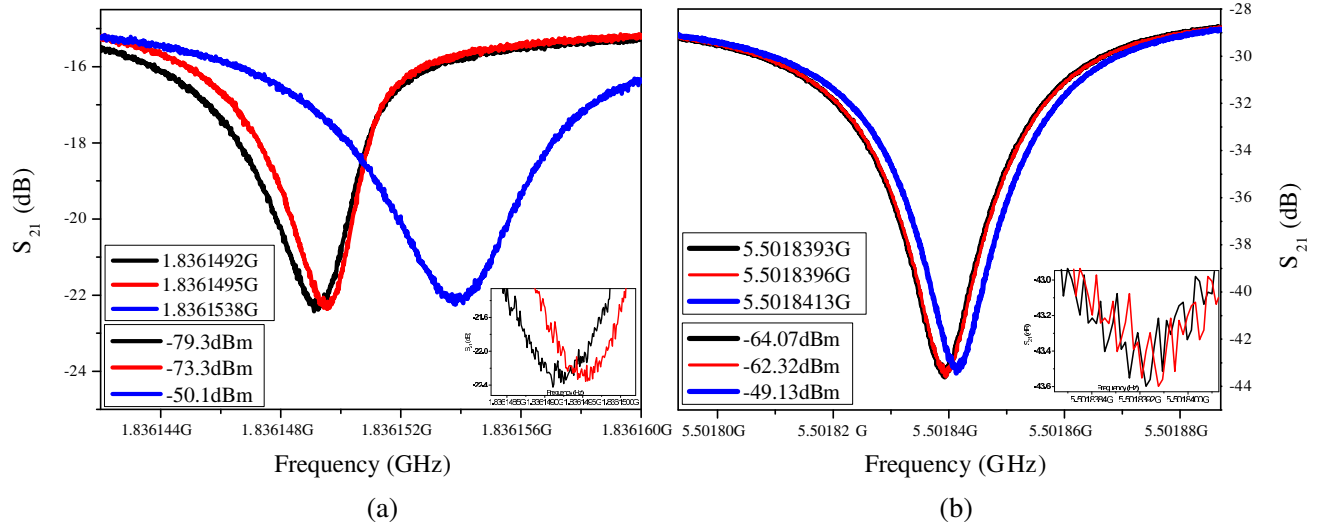


**Figure 5.** Different transmission dips respond to various irradiating light powers. (a) When the applied light is sufficiently weak, the first dip is coincidence with that without the light irradiation (the black line). Colored curves show how the center frequency of this dip shift for the light irradiations with different powers. The insert in (a) magnifies the slight responding on the center frequency shift (i.e., 300 Hz). (b) The light responding of the second dip under different irradiation powers. The insert also magnifies the 300 Hz frequency shift for the detectable weakest light (i.e.,  $-62.32$  dBm). Note that, with the increasing power of the irradiation light, both resonant dips become wider and shallower (i.e., the decreasing quality factors).

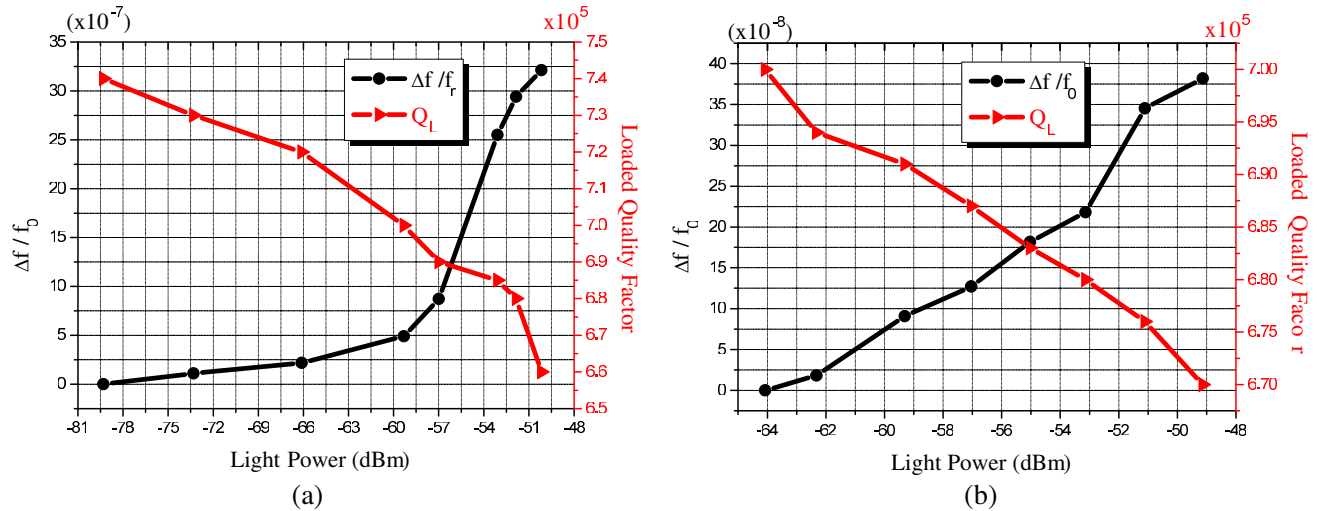


**Figure 6.** Relative shift of center frequency and the loaded quality factor versus the illuminating powers of the applied light for the first and second dips. (a) For the first dip, the central frequency shift (black line) changes with the increasing power from  $-79.3$  dBm to  $-50.1$  dBm. For such a power changing the loaded quality factor (red line) varies from  $7.4 \times 10^5$  to  $6.6 \times 10^5$ . (b) Center frequency shift of the second dip with the ascending powers from  $-64.07$  dBm to  $-49.13$  dBm (black line), and the loaded quality factor drop relevantly from  $7.0 \times 10^5$  to  $6.7 \times 10^5$  (red line).

temperature. This is checked by performing the measurements under the fixed-power light irradiation and carefully manipulating the temperature of our DR from 20 mK to 800 mK. In Fig. 7, we show how the center frequency of the first dip changes with the increase of system temperature. Here

$\Delta f = f(P, T) - f(P_0, T_0)$ , and  $f(P_0, T_0) = f_0$  stands for the measured central frequency at base temperature and the weakest light irradiation condition. It is seen that, with the increase of temperature, the center frequency shifts increase whatever with or without the light irradiation (identical with the  $-79.3$  dBm irradiation, marked as black squares). For instance, with the  $-56.9$  dBm (equals to  $2.04$  nW, marked as red circles) and  $-50.1$  dBm (equals to  $9.77$  nW, marked as green triangles) light radiation, when system temperature raises from the base  $20$  mK to  $800$  mK continuously, the center frequency shifts increase in the same tendency. Interestingly, with the increasing of system temperature, the sensitivity of the resonant frequency shifts with light irradiation decreases. Specifically, when the system temperature reaches at  $600$  mK, the center frequency shifts will not show any response to the applied light powers. This indicates that at this temperature (i.e.,  $600$  mK) the light response of the resonator is saturating to the applied incident radiations.

The above observations clearly show that, for a  $\lambda/4$  resonator working at extremely low temperature regime ( $20$  mK), the center frequencies of resonator increase with the increasing system temperature. Obviously, these behaviors are manifestly deviated from the prediction of MBT [12, 14, 15]. Based on the MBT, the resonant frequency of the resonator may also decrease under the light irradiation if the irradiation events could be served as the local heating effects. As a consequence, the relevant observations could not be explained by the standard MBT. Recently, an approach beyond the MBT has been proposed by considering the coherent effects of the quantized two-level systems [16, 21–23] on top of the resonator film due to the existence of native oxides layer [14, 16]. Practically, before the measurement, the device has to be exposed to the air environment for preparation, thus a several-nanometer-thick native oxide layer could be formed on top surface of the resonator. Phenomenally, these two-level systems possess their dipole moments and thus can couple to the around electric fields. Consequently, the dielectric constant of the film could be modified, yielding the change of central resonant frequency [24–26]. With such a two-level system model, the temperature-dependent variation of the dielectric constant for the present resonator system can be expressed as [24]

$$\frac{\Delta\epsilon}{\epsilon} = -\frac{2\delta}{\pi} \left[ \operatorname{Re}\Psi \left( \frac{1}{2} + \frac{1}{2\pi i} \frac{\hbar\omega}{k_B T} \right) - \log \frac{\hbar\omega}{k_B T} \right]. \quad (2)$$

Here,  $\omega$  is the resonant frequency of the resonator,  $\Psi$  the complex digamma function,  $k$  the Boltzmann constant, and  $\delta$  the induced dielectric loss (at  $T = 0$ ) for weak non-saturating fields. Also, the TLSs contribution to the dielectric constant could be observed as a temperature-dependent resonant frequency

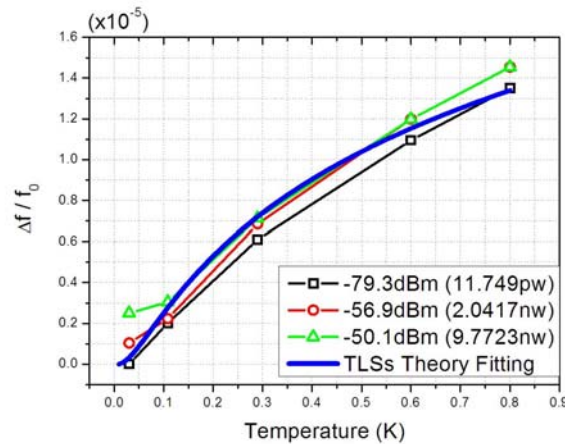


**Figure 7.** The temperature-dependent central frequency shifts  $\Delta f/f_0$  of the resonator under the irradiations with different powers, i.e.,  $P = 11.7$  pW (black squares),  $2.04$  nW (Red circles) and  $9.77$  nW (green triangles), respectively, the lines are guide to the eye. The blue line indicates the fitting result of TLSs theory, and it can be clearly found that the fitting result agrees well with the experiment data.

shift [16]:

$$\frac{\Delta f}{f_0} = -\frac{F}{2} \frac{\Delta \epsilon}{\epsilon} \quad (3)$$

where  $\Delta f = f(T) - f_0$  and  $F$  is the material filling factor. Therefore, based on the Eq. (2) we can find that at the range  $T_b > \hbar\omega/2k_B$ , the resonant frequency  $f_0$  of the resonator will increase (due to the decrease of  $\epsilon$ ) with the increasing system temperature, means that at this range, the abnormal resonant frequency shift is dominated by the TLSs (dielectric constant  $\epsilon$ ) rather than the MBT (surface inductance  $L_s$ ). We then use the Eq. (3) to numerically fit our experiment data and find they can agree well with each other, shown as the blue line in Fig. 7.

#### 4. CONCLUSION

In summary, we have set up a fiber-resonator coupling system to implement the weak light detection for the telecommunication weak light signals by using the high quality microwave resonator. At the base temperature ( $\sim 20$  mK) of our DR, we implemented the desirable light detections by probing the central frequency shift of two resonant dips. As a result, we found that the first dip is significantly sensitive to the light irradiation than the second one. Therefore, the response of the first resonant dip is more suitable for the weak light detection.

It is emphasized that the relationship between temperature (also the power of the irradiating light) and the center frequency shift of the resonator demonstrated experimentally deviated obviously from the predictions of MBT. We owe these behaviors to the coherent effects related to the two-level systems at the extremely low temperature. We have demonstrated experimentally the weak light detection in telecom-wavelength (with the significantly-low power, e.g., 35 pW) with the fabricated high- $Q$  microwave resonator at the ultra-low temperatures. In the future we will further enhance the sensitivity of the system by using lumped structure CPW resonators and adding the HEMT (High Electron Mobility Transistor amplifier) for implementing the single-photon detections [27, 28].

#### ACKNOWLEDGMENT

We thank sincerely Profs. Y. Yu, P. H. Wu, C. D. Xie, and K. C. Peng for encouragements and supports, and also Prof. C. H. Cao for help to fabricate the devices. This work is supported in part by the National Natural Science Foundation of China grant Nos. 11174373, 61301031, 91321104, U1330201, and the National Fundamental Research Program of China through Grant No. 2010CB923104.

#### REFERENCES

1. Horodecki, R., P. Horodecki, M. Horodecki, and K. Horodecki, "Quantum entanglement," *Rev. Mod. Phys.*, Vol. 81, 865–942, 2009.
2. Fukuda, D., G. Fujii, T. Numata, K. Amemiya, et al., "Titanium-based transition-edge photon number resolving detector with 98% detection efficiency with index-matched small-gap fiber coupling," *Opt. Express*, Vol. 19, No. 2, 870–875, 2011.
3. Namekata, N., Y. Takahashi, G. Fujii, D. Fukuda, et al., "Non-Gaussian operation based on photon subtraction using a photon-number-resolving detector at a telecommunications wavelength," *Nature Photonics*, Vol. 4, 655–660, 2010.
4. Ekert, A. K., "Quantum cryptography based on Bells theorem," *Phys. Rev. Lett.*, Vol. 67, 661–663, 1991.
5. Goltsman, G. N., O. Okunev, G. Chulkova, A. Lipatov, et al., "Picosecond superconducting single-photon optical detector," *Appl. Phys. Lett.*, Vol. 79, No. 6, 705–707, August 2001.
6. Eisenmenger, W., *Superconducting Tunnelling Junctions as Phonon Generators and Detectors*, 2010.
7. Irwin, K. D., "An application of electrothermal feedback for high resolution cryogenic particle detection," *Appl. Phys. Lett.*, Vol. 66, April 1995.

8. Lita, A. E., A. J. Miller, and S. W. Nam, "Counting near-infrared single-photons with 95% efficiency," *Opt. Express*, Vol. 16, 3032–3040, 2008.
9. Day, P. K., H. G. LeDuc, B. A. Mazin, A. Vayonakis, and J. Zmuidzinas, "A broadband superconducting detector suitable for use in large arrays," *Nature*, Vol. 425, 817–821, October 2003.
10. Mazin, B. A., B. Bumble, and P. K. Day, "Position sensitive x-ray spectrophotometer using microwave kinetic inductance detectors," *Appl. Phys. Lett.*, Vol. 89, No. 22, 222507, 2006.
11. Noroozian, O., P. K. Day, B. H. Eom, H. G. LeDuc, et al., "Crosstalk reduction for superconducting microwave resonator arrays," *IEEE Trans. Microw. Theory Tech.*, Vol. 60, No. 5, May 2012.
12. Mattis, D. C. and J. Bardeen, "Theory of the anomalous skin effect in normal and superconducting metals," *Phys. Rev.*, Vol. 111, 412–417, 1958.
13. Tinkham, M., *Introduction to Superconductivity*, 2nd edition, McGraw-Hill, New York, 1996.
14. Barends, R., J. J. A. Baselmans, J. N. Hovenier, J. R. Gao, et al., "Niobium and Tantalum high  $Q$  resonators for photon detectors," *IEEE Trans. Appl. Supercond.*, Vol. 17, 263, 2007.
15. Quaranta, O., T. W. Cecil, and A. Miceli, "Tungsten silicide alloys for microwave kinetic inductance detectors," *IEEE Trans. Appl. Supercond.*, Vol. 23, No. 3, 2400104, June 2013.
16. Gao, J. S., M. Daal, A. Vayonakis, S. Kumar, et al., "Experimental evidence for a surface distribution of two-level systems in superconducting lithographed microwave resonators," *Appl. Phys. Lett.*, Vol. 92, 152505, 2008.
17. Li, H. J., Y. W. Wang, L. F. Wei, P. J. Zhou, et al., "Experimental demonstrations of high- $Q$  superconducting coplanar waveguide resonators," *Chinese Sci. Bull.*, Vol. 58, No. 1, 1–5, 2012.
18. Hammer, G., S. Wuensch, M. Roesch, K. Ilin, et al., "Coupling of microwave resonators to feed lines," *IEEE Trans. Appl. Supercond.*, Vol. 19, No. 3, June 2009.
19. Mazin, B. A., *Microwave Kinetic Inductance Detectors*, 2005.
20. Ponchak, G. E., J. Papapolymerou, and M. M. Tentzeris, "Characterization of liquid crystal polymer (LCP) material and transmission lines on LCP substrates from 30 to 110 GHz," *IEEE Trans. Microw. Theory Techn.*, Vol. 53, No. 713, 2005.
21. Kumar, S., J. S. Gao, J. Zmuidzinas, B. A. Mazin, et al., "Temperature dependence of the frequency and noise of superconducting coplanar waveguide resonators," *Appl. Phys. Lett.*, Vol. 92, 123503, 2008.
22. Wisbey, D. S., J. S. Gao, M. R. Vissers, F. C. S. da Silva, et al., "Effect of metal/substrate interfaces on radio-frequency loss in superconducting coplanar waveguides," *J. Appl. Phys.*, Vol. 108, 093918, 2010.
23. Khalil, M. S., F. C. Wellstood, and K. D. Osborn, "Loss dependence on geometry and applied power in superconducting coplanar resonators," *IEEE Trans. Appl. Supercond.*, Vol. 21, No. 3, June 2011.
24. Phillips, W. A., "Two-level states in glasses," *Rep. Prog. Phys.*, Vol. 50, 1657–1708, 1987.
25. Phillips, W. A., "Tunneling states in amorphous solids," *J. Low Temp. Phys.*, Vol. 7, 351, 1972.
26. Anderson, P. W., B. I. Halperin, and C. M. Varma, "Anomalous low-temperature thermal properties of glasses and spin glasses," *Philos. Mag.*, Vol. 25, No. 1, 1972.
27. Gao, J., M. R. Vissers, M. O. Sandberg, F. C. S. da Silva, et al., "A titanium-nitride near-infrared kinetic inductance photon-counting detector and its anomalous electrodynamics," *Appl. Phys. Lett.*, Vol. 101, 142602, 2012.
28. Wuensch, S., R. Prinz, C. Groetsch, and M. Siegel, "Optimized microwave LEKID arrays for high-resolution applications," *IEEE Trans. Appl. Supercond.*, Vol. 23, No. 3, June 2013.